

Study of Circular Dichroism Modes Through Decomposition of Planar Nanostructures

W. K. Phua^{1,2} · Y. L. Hor¹ · Eunice S. P. Leong³ · Y. J. Liu³ · E. H. Khoo^{1,2}

Received: 8 June 2015 / Accepted: 14 August 2015 / Published online: 29 August 2015
© Springer Science+Business Media New York 2015

Abstract We extend the plasmon hybridization method from a single nanoparticle to a complex planar nanostructure, decomposing the complex nanostructure into fundamental nanoparticle building blocks. Using gammadion nanostructure as an example, we validated the theory by comparing the field profile in the gammadion's arms under the influence of an incident circularly polarized wave. This allows us to address the origin of the plasmonics modes in the circular dichroism (CD) spectrum. The use of this hybridization method provides a simple and intuitive explanation on how conductive and inductive coupling may result from complex planar nanostructures, allowing us to study its optical properties. Using our approach, top down hybridization studies can be applied to other complex planar structures to gain further insight on the origin of the CD modes and enhance ultrasensitive sensing of chiral micro and macro molecules.

Keywords Circular dichroism · Hybridization · Plasmons · Planar

Introduction

To probe the conformational state of biomolecules, chiral optical techniques such as circular dichroism (CD) [1] are the most popular due to its allowance for rapid detection, small sample volume, simple experimental setup and low equipment cost [2]. CD refers to the absorption difference between left-handed (LCP) and right-handed (RCP) circularly polarized light in chiral materials and biomolecules. The difference in absorption stems from the preference of chiral materials and biomolecules to absorb light waves that are of opposite handedness.

The interaction between light waves and biomolecules is very weak, resulting in weak CD signals [3]. To overcome this problem, researchers proposed localized surface plasmon resonance (SPR) [4] to enhance interaction between biomolecules and light waves [5]. This increases the absorption difference of LCP and RCP and, therefore, CD. The utilization of plasmonics increases the number of peaks observed in the CD spectrum, made possible due to plasmon excitations interacting with the dipoles of the engineered structure.

Asymmetrical nanostructures have been used in chirality studies to enhance the sensitivity of biomolecule detection and CD spectrum signal [4–7]. A commonly used asymmetrical nanostructure is the gammadion. One reported work demonstrated an improvement in sensitivity by a factor of order 6 [4]. However, these reports do not provide an in-depth explanation on the origin of the modes in the CD spectra which is important in providing useful information for chirality detection. To study the origin of its CD modes, we adopted the plasmon hybridization method which describes how plasmons [4] from metal nanostructures interact with one another, forming different energy states and hence inducing different behaviours at the plasmon resonance frequencies [8]. The method is well suited for use on the gammadion nanostructure due to its

✉ E. H. Khoo
khooeh@ihpc.a-star.edu.sg

¹ A*STAR Institute of High Performance Computing, 1 Fusionopolis Way, #16-16 Connexis, Singapore 138632, Singapore

² Department of Electrical and Computer Engineering, National University of Singapore, 21 Lower Kent Ridge Road, Singapore 119077, Singapore

³ A*STAR Institute of Materials Research and Engineering, 3 Research Link, Singapore 117602, Singapore

asymmetric shape and its ease of being decomposed into basic nanoparticle building blocks. It is important to note that while CD is due to the asymmetric shape of gammadion, the presence of the modes and their characteristics require a deeper understanding of the physics.

Plasmon hybridization provides a simple and intuitive explanation behind the interaction of plasmons supported by elementary nanostructures, namely nanosphere, nanorice and nanostar [8–10]. The theoretical formalism [11, 12] was applied to the interaction between nanosphere and surface [13]. There were also studies on new plasmon mode creation when two nanoparticles are placed close together to form a nanoparticle pair [14, 15].

Theory and Modeling

In this paper, the objective is to apply the plasmon hybridization method to investigate the different modes in the CD spectra of the gammadion nanostructure as a result of optical excitation by circularly polarized waves. While one would expect the largest wavelength shift for the mode that exhibits the largest CD, this is contrary to what has been observed [4], whereby a smaller CD signal may induce a reasonably large wavelength shift. For biosensing applications, an increase in wavelength shift results in enhanced sensitivity which is what we hope to achieve. Hence, there is a need to study the physics of two modes in more detail using the hybridization method.

As an individual unit, the planar gammadion nanostructure exhibits chiral handedness. Since the fundamental building blocks of the gammadion can be easily identified, it serves as a good candidate for plasmon hybridization studies, allowing structural decomposition for easy analysis. The methodology can be validated against other simulations or experimental results. Hybridization studies allow the field distributions to be shown, allowing for the identification of different modes for a particular structure. Contrary to other studies on resonance

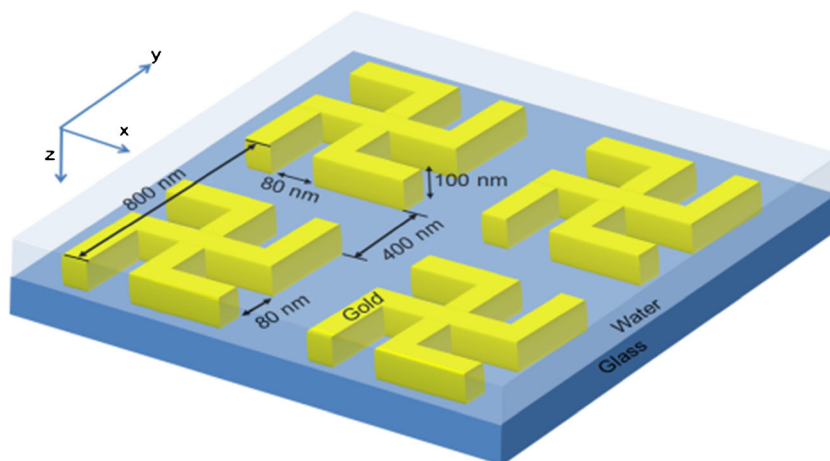
modes [5], this study utilizes the decomposition of a single planar gammadion nanostructure into smaller fundamental nanoparticle elements so as to analyze the field distribution. The interaction of the induced dipole moments between adjacent/neighbouring nanoparticle elements makes up the overall induced dipole moment for the entire nanostructure. We apply fundamental physics of local charge distribution to provide an intuitive picture on how hybridized plasmon modes arise. The conductive and inductive coupling that results in the gammadion nanostructure forms the hybridized plasmon modes in the CD spectrum. The effects of different modes for sensing chiral molecules are discussed using field distribution, Bloch wave theory and charge distribution, thereby explaining the origin of the CD modes.

We have selected the left-handed gammadion structure shown in Fig. 1 to apply the plasmon hybridization method and study the origin of the CD modes. Such configuration facilitates fabrication and usage in liquid medium for biosensing applications.

Similar concepts can be applied to the right-handed gammadion structure as well. We first consider the incidence of RCP light on the left-handed gammadion structure. There is a rotation in the polarization of light from the E_y direction to the E_x direction as shown in Fig. 2. Due to the rotational symmetry of the gammadion structure, the dominant polarization is along the x and y direction. Since CD is based on the difference in absorption between the LCP and RCP light, we need to consider the differences between two linearly polarized waves that contribute to the circular rotation of the waves. Assuming that the E_x polarized wave is 90° out of phase with the E_y polarized wave for the RCP and negative 90° out of phase for the LCP, we set E_y polarization as the reference. Hence, the E_x polarized waves of the LCP and RCP have a phase difference of 180° .

We need to consider the impact of induced dipole moments from E_x polarization, $-E_x$ polarization and E_y polarization. Defining an electric dipole moment in the configuration

Fig. 1 Schematic layout of the left-handed gammadion structure. Left/right circular polarized wave is incident in the z direction into the planar array



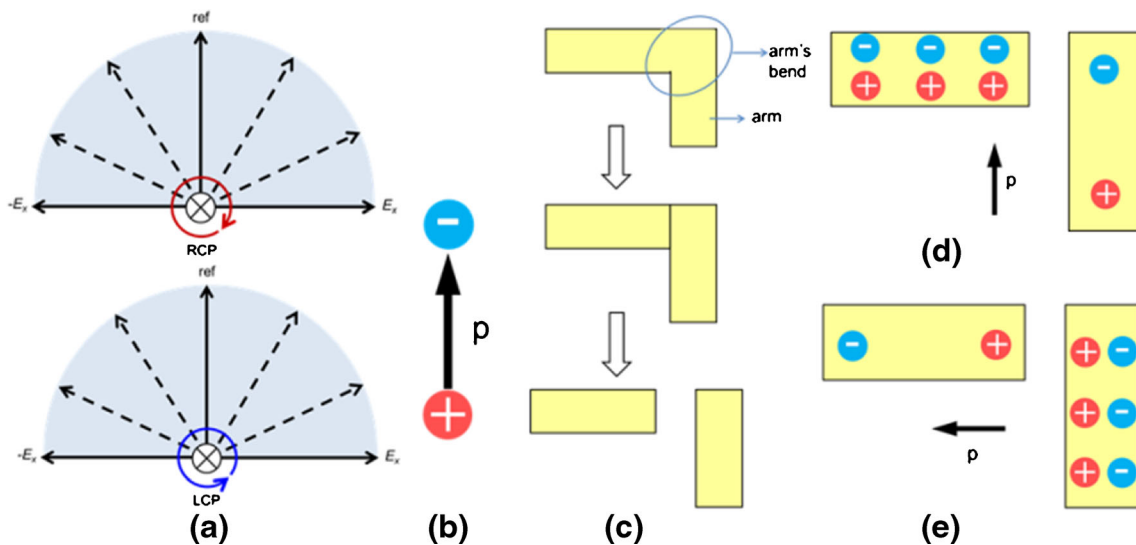


Fig. 2 **a** Rotation in light orientation for RCP and LCP, with light normally incident onto the xy -plane. *Dotted lines* indicate the field components in the xy -plane. **b** Charge distribution for electric dipole. **c** Dissection of Gammadion's arm and arm's bend. **d** Electric dipole

moment induced in a single nanowire with E_y light polarization. **e** Electric dipole moment induced in a single nanowire with $-E_x$ light polarization

shown in Fig. 2b [15], the gammadion structure is dissected into several nanowire structures shown in Fig. 2c. We label the gammadion's arm and arm's bend. It is planar where the arms and arms' bend are interconnected. When we consider a single nanowire of subwavelength dimensions, we can excite an electric dipole moment in the nanowire with an incident light source of known polarization. Different dipole moments will be induced depending on the polarization of the excitation light source. Figure 2d, e shows two nanowire structures and their dipole moments induced with E_y and $-E_x$ light polarization, respectively.

The derived charge distribution at each arm and arm's bend of the gammadion is shown in Fig. 3a–c. Both x and y polarizations lead to distinct dipole charge moments in the arms and arms' bend. We consider RCP to be a superposition of E_y and E_x polarized waves while LCP is the superposition of E_y and $-E_x$ polarized waves. As a result of RCP and LCP, two hybridization states can be attained through the superposition of the dipole moments in the E_y and E_x polarization as well as E_y and $-E_x$ polarization, respectively. This allows us to derive the resultant dipole moments, otherwise known as polarization as shown in Fig. 3d, e. Since we use the y direction as the reference direction for light polarization, we expect two other corresponding hybridization states (Fig. 3f, g). These two hybridized states are a result of opposite field polarity at the arms of the gammadion, derived as a result of charge cancellations due to superposition.

Results and Discussion

The gammadion structure shown in Fig. 1 has a width of 80 nm and a periodicity of 800 nm. It is 100 nm thick, placed

on glass substrate and surrounded by water. We use gold for the gammadion because it does not oxidize, is chemically inert and is biologically compatible. The permittivity values of glass, water and gold are obtained from the optical handbook [16]. The gammadion was simulated using the finite-difference time-domain (FDTD) method with Lorentz-Drude

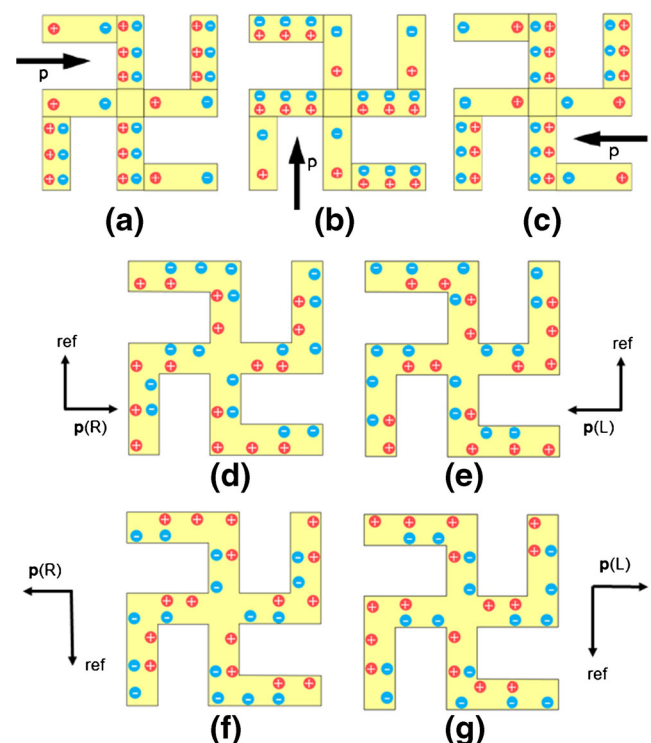


Fig. 3 Electric dipole moment induced in a single gammadion nanostructure with **a** E_x , **b** E_y and **c** $-E_x$ light polarization. **d** Hybridization state 1 with RCP. **e** Hybridization state 1 with LCP. **f** Hybridization state 2 with RCP. **g** Hybridization state 2 with LCP

model to account for the damping of the metal. We use periodic boundary conditions to account for the gammadion array and apply perfectly matched layer to the vertical axis of the array. The simulation grid size is set to 4 nm in all directions to obtain accurate transmission, scattering and reflection spectra. We obtained the absorption spectra of the gammadion using left- and right-handed circular polarized light and take the difference, giving us the CD spectrum as shown in Fig. 4a. The CD of the gammadion is given as

$$CD = A_L - A_R \quad (1)$$

where A_L/A_R refers to the absorption of LCP/RCP, respectively. Since the gammadion is a left-handed structure, it is expected that more right-handed circular polarized light is absorbed [17]. This is due to the electric field vector of the right-handed circularly polarized light having stronger interactions with the induced electric dipole moments of the left-handed gammadion structure. Hence, the CD of the gammadion array is negative at the visible light spectrum, as calculated from Eq. 1.

From Fig. 4a, there are three distinctive CD modes m1, m2 and m3 corresponding to valleys observed at wavelengths of 751, 578 and 524 nm, respectively. Mode m1 has the largest CD, while mode m2 and m3 are close to each other and have smaller CD values. Figure 4b shows the normalized E_z field distribution of the three modes. We observed that mode m1 has the largest field distribution spread compared to modes m2 and m3. Mode m1 also shows stronger electric field intensity near the edges of the gammadion. Field distribution is used to

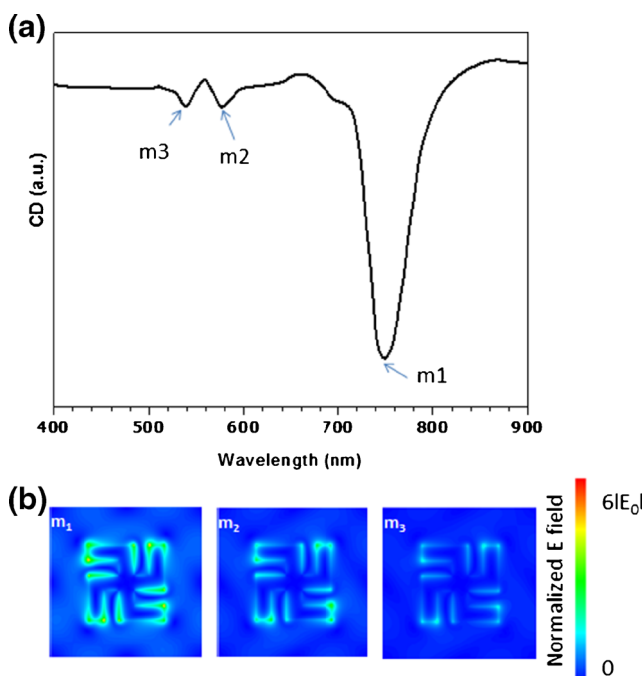


Fig. 4 **a** Modes obtained from gammadion structure. Mode m1 correspond to Bloch mode while modes m2 and m3 are localized plasmonics modes. **b** Normalized E field distribution of the three modes

investigate the origin of the CD modes. The large and intense field distribution in mode m1 is a result of the interaction between adjacent gammadion structures in a collective array. Secondly, mode m1 is located near the period. The mode arising from the period of the gammadion is given as

$$\lambda_{SPP} = \frac{n_{SPP} a_0}{\sqrt{2}} \quad (2)$$

where a_0 is the period of the structure, n_{SPP} and λ_{SPP} is the effective index and wavelength of the surface plasmon, respectively.

Figure 5 shows the CD spectra with different periods. It is observed that mode m1 blue shifted from 755 to 645 nm as the period is reduced from 800 to 700 nm. This demonstrates that mode m1 is dependent on the period of the gammadion array and we label it as the plasmonics CD Bloch mode [18].

Modes m2 and m3 are near each other and have similar CD. Their CD is smaller in amplitude because of the inductive and conductive coupling in each individual gammadion nanostructure [19]. In addition, the field distribution is localized onto a very small field spread on the gammadion/water interface. We deduced that modes m2 and m3 originate from localized surface modes with different polarity distributions. Plotting the dipolar field profile for mode m2 as shown in Fig. 6a, b, we observe that the regions of maxima and minima field intensity are congregated around the edges, particularly at the regions whereby the adjacent arms are in close proximity to each other. Only fields that are oriented in the z direction are plotted in this figure. There is strong coupling between positive and negative poles, resulting in enhanced local electric field intensity. Similar features can be observed from mode m3 as well, with its field plots and corresponding schematic being shown in Fig. 6c, d, respectively.

The E field profile of mode m2 hybridized state with RCP and LCP exhibits a polarity profile in the arms and arms' bend

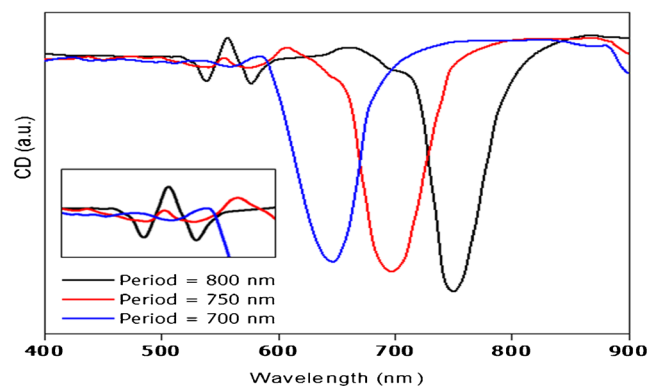
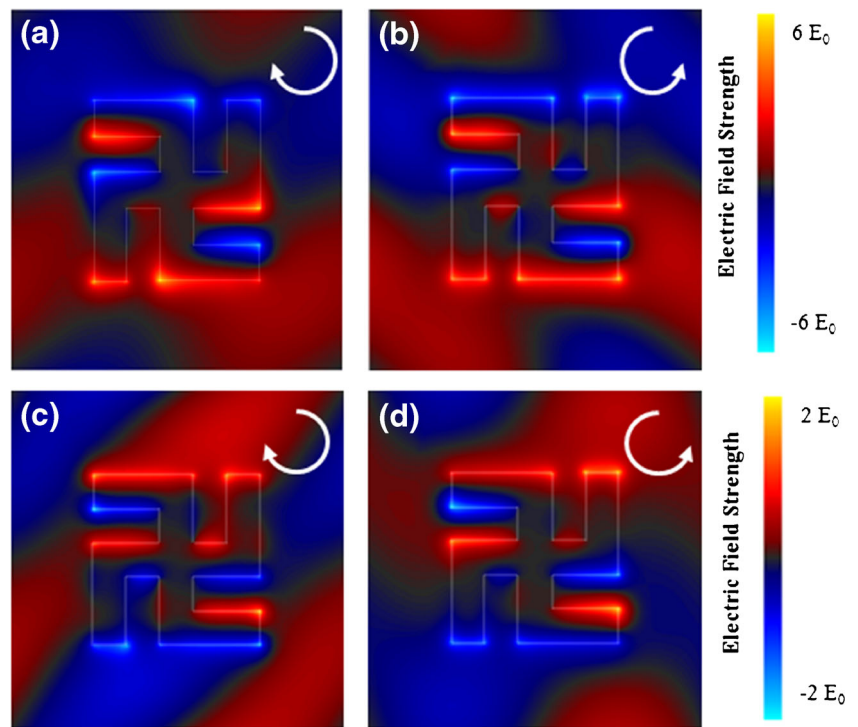


Fig. 5 Blue shift (Bloch mode effect) in spectrum of mode m1 with a decrease in structure periodicity

Fig. 6 *E* field profile. **a** Mode m2 RCP hybridized state. **b** Mode m2 LCP hybridized state. **c** Mode m3 RCP hybridized state. **d** Mode m3 LCP hybridized state



that is inversely related to the m3 hybridized state with RCP and LCP. The pair of modes, m2 and m3, is the result of the presence of a mixture of inductive and conductive coupling, respectively, as termed in [15]. As discussed, hybridization can be defined as the formation of different energy states as a result of interactions resulting from both inductive and conductive coupling [8]. The *E* field profile for modes m2 and m3 shown in Fig. 6a–d resembles the derived electric dipole moments in Fig. 3d–g. This strong agreement further augments the validity of applying plasmon hybridization method on complex nanostructures.

Hence, we can define modes m2 and m3 as hybridized modes. Inductive coupling occurs as a result of coupling of dipoles between the arms and their adjacent arms’ bends while conductive coupling refers to the coupling of resultant dipoles in the structure. Within the gammadion, there exists not just coupling between purely two transverse or two longitudinal dipoles but also coupling between a transverse and longitudinal dipole. Interaction energy between two purely transverse/longitudinal dipoles [15] is given by

$$H_{\text{int}} = \gamma \frac{p_1 p_2}{4\pi\epsilon_0 r^3} \tag{3}$$

where $p_{1,2}$ are dipole moments and r is the distance away from the interaction centre. Parameter γ is called the interaction index and can be assigned +1 or –2, depending on whether it is a transverse or longitudinal

coupling. H_{int} between a transverse and longitudinal dipole [Appendix] is derived to be

$$H_{\text{int}} = \frac{\left(\frac{3}{2}d\right)p_1 p_2}{4\pi\epsilon_0 r^4} \tag{4}$$

γ has a value of $3d/2r$ and is dependent on r . This means that H_{int} decreases to zero more rapidly for coupling between longitudinal and transverse dipoles than coupling between two purely transverse/longitudinal dipoles. Apart from the merging of the partial charges of the dipoles as r increases, the reason for the rapid decrease in H_{int} is due to the increased separation of the charges on the far ends of the longitudinal and transverse dipole. This rapid decrease of H_{int} affects the strength of the CD signal for both modes m2 and m3. Earlier, Fig. 3d, e shows the sign distribution of the whole gammadion structure. The polarity of the field at the arm and arm’s bend of the gammadion determine the nature of the modes in the absorption spectrum. This subsequently affects the nature of the modes in the CD spectrum. Mode m2 lies at a higher resonance wavelength (578 nm) than mode m3 (524 nm). The different polarity profiles for m2 and m3 hybridized state with LCP and RCP explain why the CD modes m2 and m3 are at different wavelengths.

Hence, by changing the gap distance between the arm and the adjacent arm’s bend of the gammadion, the CD of modes

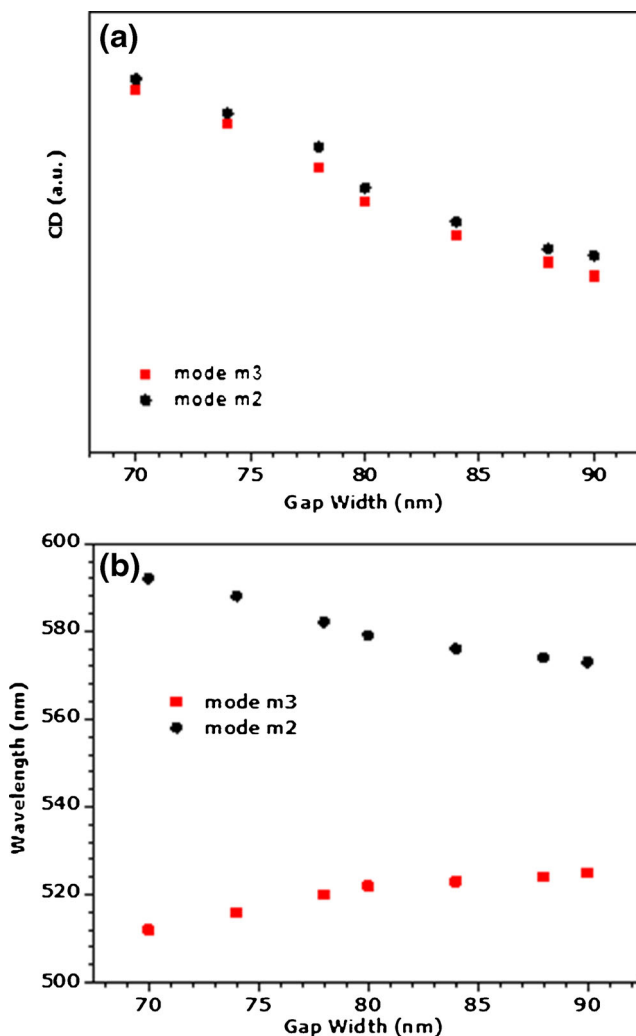


Fig. 7 a CD plot for modes m2 and m3 with various gap widths. b Wavelength shift of mode m2 and m3 with various gap widths

m2 and m3 will change. In Fig. 7a, we observed that the CD magnitude of mode m2 and m3 decreases as the gap increases from 70 to 90 nm. This is due to weaker inductive coupling between dipoles on the adjacent arms. In Fig. 7b, the wavelength of mode m2 blue and m3 red shifted. The weakened interaction between the dipoles causes the energy difference between the two hybridization states to decrease, hence decreasing the wavelength difference between modes m2 and m3 simultaneously. On the other hand, decreasing the gap distance causes stronger inductive coupling. The stronger interaction results in a larger energy difference between the two hybridization states and causes a higher wavelength difference between modes m2 and m3. We also observed a larger CD for m2 and m3.

Since mode hybridization occurs simply because of inductive and conductive coupling, this means a single structure can support more than one hybridization mode.

Also, from the field intensity plots, mode m2 is seen to give slightly stronger CD signal than mode m3. This in turn infers a stronger absorption for mode m2 than mode m3 and hence a stronger CD. Since mode m2 occurs at a higher wavelength than mode m3, this means that there is a higher probability of absorption at higher wavelength, cumulating in the stronger CD signal attained.

In theory, the hybrid modes of m2 and m3 in CD spectrum can be explained using the Born-Kuhn oscillation model for optical activity. The arm and arm's bend of the gammadion can be approximated by two harmonic oscillators [20], which give rise to inductive and conductive coupling. Hence, as the distance between the arm and arm's bend increases, we see that the coupling weakens [19]. By using Maxwell equation for dispersive dielectric material, $D = \epsilon_0 E + P$, the Born-Kuhn model gives two solutions for the average refractive index of the chiral gammadion with LCP and RCP light incidence. We use the two electron chiral molecule oscillation model and consider nonlocality of the first order dispersion [21]. The solutions to the Born-Kuhn oscillation model is given as

$$\omega_{2,3}^2 = \omega_0^2 + \xi \quad (5)$$

where the subscripts refer to modes m2 and m3. The parameter ω_0 is the natural frequency of the oscillation pair (or the CD hybrid modes) and ξ is the coupling between arm and arm's bend. As the gammadion is asymmetrical, the coupling between the arm and arm's bend is different, thereby giving rise to the shift in wavelength as shown in Fig. 7b.

Conclusions

We have utilized the plasmon hybridization method to investigate the origin of CD modes in metallic gammadion nanostructures. The largest CD mode is mode m1, which originated from periodic Bloch modes of the gammadion array. Modes m2 and m3 are caused by both inductive and conductive coupling. Finally, we varied the gap distance between the arm and the adjacent arm's bend to investigate the effects of inductive coupling on CD modes. The knowledge of CD modes allows us to design nanostructures that facilitate and optimize localized plasmon modes with desired electromagnetic field profile. Realizing chiroptically selective nanostructures allows applications in biosensors and chiral photochemical catalysts.

Acknowledgments We acknowledge the support of this research by A*STAR Joint Council Office with Grant #12302FG012. We also

acknowledge the financial support from Scientific Staff Development Award, A*STAR Institute of High Performance Computing, Singapore.

Appendix

Correlation of Mode m1 with Period of the Gammadion Array, a_0

The period of the gammadion array, a_0 is varied in the equation [18].

$$\lambda_{\text{SPP}} = \frac{n_{\text{SPP}} a_0}{\sqrt{n^2 + m^2}} \tag{6}$$

Since our structure is only fundamental, we only consider the fundamental SPP modes. For fundamental SPP modes, $n = m = 1$ for the mode on the gammadion. The effective localized surface plasmon is given as

$$n_{\text{SPP}} = \sqrt{\frac{\epsilon_{\text{Au}} \epsilon_d}{\epsilon_{\text{Au}} + \epsilon_d}} \tag{7}$$

We plot the graph of Eq. 6 with the wavelength positions of mode m1 in the CD spectra for different periods of the gammadion array. We simulate the gammadion array with periods of 850, 800, 750, 700 and 650 nm. Figure 8 shows the comparison between the model and simulation results.

From Fig. 8, we observed that Eq. 6 and the wavelength positions of mode m1 in CD spectra match excellently.

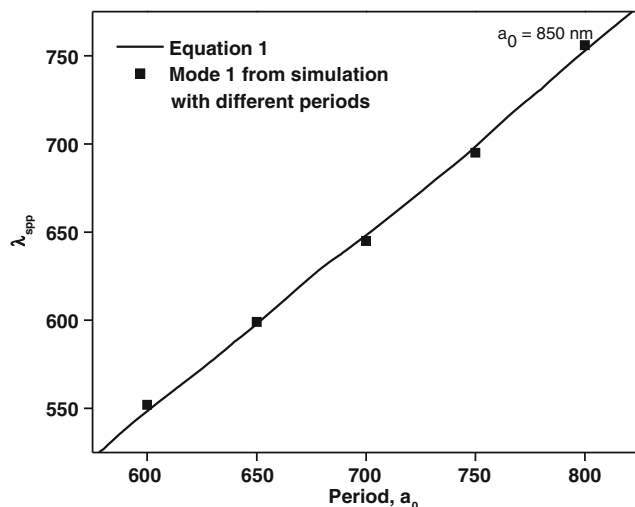
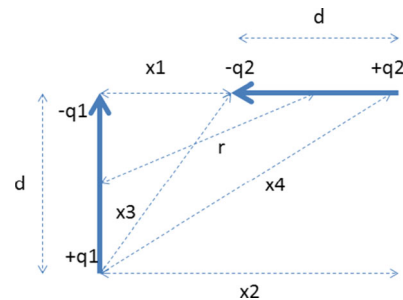


Fig. 8 Plot of the Eq. 6 and mode 1 from CD spectra

Calculation of Potential/Interaction Energy, U Between a Transverse Dipole and a Longitudinal Dipole to Account for Conductive Coupling in a Gammadion Structure

Circularly polarized light involves the superposition of both E_x and E_y polarized waves, assuming that the wave propagates in the z direction. Hence, it requires the consideration of both longitudinal and transverse coupling.

We can represent the transverse dipole as a separation of positive and negative charge $+q_1$ and $-q_1$, respectively. Similarly, the longitudinal dipole can be considered as a separation of positive and negative charge $+q_2$ and $-q_2$, respectively. Hence, the interaction energy, U , can be represented as follows, whereby $\frac{1}{4\pi\epsilon_0}$ refers to the electrostatic constant. We have also defined x_1 to be the distance between $-q_1$ and $-q_2$, x_2 to be the distance between $-q_1$ and $+q_2$, x_3 to be the distance between $+q_1$ and $-q_2$ and x_4 to be the distance between $+q_1$ and $+q_2$.



$$U = \frac{1}{4\pi\epsilon_0} \left[\frac{(-q_1)(-q_2)}{x_1} + \frac{(-q_1)q_2}{x_2} + \frac{q_1(-q_2)}{x_3} + \frac{q_1q_2}{x_4} \right]$$

$$= \frac{q_1q_2}{4\pi\epsilon_0} \left(\frac{1}{x_1} - \frac{1}{x_2} - \frac{1}{x_3} + \frac{1}{x_4} \right)$$

We need to obtain values for x_1, x_2, x_3 and x_4 . Using the Pythagoras theorem,

$$\left(x_1 + \frac{d}{2}\right)^2 + \left(\frac{d}{2}\right)^2 = r^2$$

$$x_1 = \sqrt{r^2 - \left(\frac{d}{2}\right)^2} - \frac{d}{2} = r \left(\sqrt{1 - \left(\frac{d}{2r}\right)^2} - \frac{d}{2r} \right) \tag{8}$$

$$x_2 = x_1 + d = r \left(\sqrt{1 - \left(\frac{d}{2r}\right)^2} - \frac{d}{2r} \right) + d$$

$$= r \left(\sqrt{1 - \left(\frac{d}{2r}\right)^2} + \frac{d}{2r} \right) \tag{9}$$

$$\begin{aligned}
 x_3^2 &= d^2 + x_1^2 = d^2 + \left(\sqrt{r^2 - \left(\frac{d}{2}\right)^2} - \frac{d}{2} \right)^2 = d^2 + r^2 - \left(\frac{d}{2}\right)^2 - d\sqrt{r^2 - \left(\frac{d}{2}\right)^2} + \left(\frac{d}{2}\right)^2 = d^2 + r^2 - d\sqrt{r^2 - \left(\frac{d}{2}\right)^2} \\
 x_3 &= \sqrt{d^2 + r^2 - d\sqrt{r^2 - \left(\frac{d}{2}\right)^2}} = r \sqrt{\left(\frac{d}{r}\right)^2 + 1 - \frac{d}{r}\sqrt{1 - \left(\frac{d}{2r}\right)^2}}
 \end{aligned} \tag{10}$$

$$\begin{aligned}
 x_4^2 &= d^2 + x_2^2 = d^2 + \left(\sqrt{r^2 - \left(\frac{d}{2}\right)^2} + \frac{d}{2} \right)^2 = d^2 + r^2 - \left(\frac{d}{2}\right)^2 + d\sqrt{r^2 - \left(\frac{d}{2}\right)^2} + \left(\frac{d}{2}\right)^2 = d^2 + r^2 + d\sqrt{r^2 - \left(\frac{d}{2}\right)^2} \\
 x_4 &= \sqrt{d^2 + r^2 + d\sqrt{r^2 - \left(\frac{d}{2}\right)^2}} = r \sqrt{\left(\frac{d}{r}\right)^2 + 1 + \frac{d}{r}\sqrt{1 - \left(\frac{d}{2r}\right)^2}}
 \end{aligned} \tag{11}$$

To simplify the expression, let $x = \frac{d}{r}$

$$x_1 = r(\sqrt{1-x^2}-x) \tag{12}$$

$$x_2 = r(\sqrt{1-x^2}+x) \tag{13}$$

$$x_3 = r\sqrt{(2x)^2 + 1 - 2x\sqrt{1-x^2}} = r\sqrt{4x^2 + 1 - 2x\sqrt{1-x^2}} \tag{14}$$

$$x_4 = r\sqrt{4x^2 + 1 + 2x\sqrt{1-x^2}} \tag{15}$$

Using Taylor series expansion,

$$\frac{1}{x_1} \approx \frac{1}{r} \left\{ 1 + x + \frac{3}{2}x^2 + 2x^3 + \frac{23}{8}x^4 + O(x^5) \right\} \tag{16}$$

$$\frac{1}{x_2} \approx \frac{1}{r} \left\{ 1 - x + \frac{3}{2}x^2 - 2x^3 + \frac{23}{8}x^4 + O(x^5) \right\} \tag{17}$$

$$\frac{1}{x_3} \approx \frac{1}{r} \left\{ 1 + x - \frac{1}{2}x^2 - 4x^3 - \frac{49}{8}x^4 + O(x^5) \right\} \tag{18}$$

$$\begin{aligned}
 \frac{1}{x_4} &\approx \frac{1}{r} \left\{ 1 - x - \frac{1}{2}x^2 + 4x^3 - \frac{49}{8}x^4 + O(x^5) \right\} \\
 U &= \frac{q_1 q_2}{4\pi\epsilon_0} \left(\frac{1}{x_1} - \frac{1}{x_2} - \frac{1}{x_3} + \frac{1}{x_4} \right) \approx \frac{q_1 q_2}{4\pi\epsilon_0 r} (12x^3)
 \end{aligned} \tag{19}$$

$$U \approx \frac{q_1 q_2}{4\pi\epsilon_0 r} 12 \left(\frac{d}{2r}\right)^3 \approx \frac{\left(\frac{3}{2}\right) dq_1 dq_2 d}{4\pi\epsilon_0 r^4} \approx \frac{\left(\frac{3}{2}d\right) p_1 p_2}{4\pi\epsilon_0 r^4}$$

where $p_1 = q_1 d$ and $p_2 = q_2 d$
 $p_{1,2}$ = dipole moment of 1,2

Relation Between Energy Difference and Wavelength Difference

$$\begin{aligned}
 E &= \frac{hc}{\lambda} \\
 \frac{\partial E}{\partial \lambda} &= -\frac{hc}{\lambda^2} \\
 \partial \lambda &= -\frac{\lambda^2}{hc} \partial E
 \end{aligned}$$

When ∂E decreases, $\partial \lambda$ decreases as well.

References

1. Fasman GD (1996) Circular dichroism and the conformational analysis of biomolecules. Plenum US, New York
2. Greenfield NJ (2007) Using circular dichroism spectra to estimate protein secondary structure. Nat Protoc 1:2876
3. Correa DHA, Ramos CHI (2009) The use of circular dichroism spectroscopy to study protein folding, form and function. Afr J Biochem Res 3(5):164
4. Hendry E, Carpy T, Johnston J, Popland M, Milhaylovskiy RV, Laphom AJ, Kelly SM, Barron LD, Gadegaard N, Kadodwala M (2010) Ultrasensitive detection and characterisation of biomolecules using superchiral fields. Nat Nanotechnol 5:783
5. Zhao R, Zhang L, Zhou J, Koschny T, Soukoulis CM (2011) Conjugated gammadion chiral metamaterial with uniaxial optical activity and negative refractive index. Phys Rev B 83:035105
6. Rogacheva AV, Fedotov VA, Schwanecke AS, Zheludev NI (2006) Giant gyrotropy due to electromagnetic coupling. Phys Rev Lett 97: 177401
7. Decker M, Klein MW, Wegener M, Linden S (2007) Circular dichroism of planar chiral magnetic metamaterials. Opt Lett 32(7): 856

8. Prodan E, Radloff C, Halas NJ, Nordlander P (2003) A hybridization model for the plasmon response of complex nanostructures. *Science* 302:419
9. Wang H, Brandl DW, Le F, Nordlander P, Halas NJ (2006) Nanorice: a hybrid plasmonic nanostructure. *Nano Lett* 6:827
10. Hao F, Nehl CL, Hafner JH, Nordlander P (2007) Plasmon resonances of a gold nanostar. *Nano Lett* 7(3):729
11. Prodan E, Nordlander P (2004) Plasmon hybridization in spherical nanoparticles. *J Chem Phys* 120(11):5444
12. Bao K, Sobhani H, Nordlander P (2010) Plasmon hybridization for real metals. *Chin Sci Bull* 55(24):2629
13. Nordlander P, Prodan E (2004) Plasmon hybridization in nanoparticles near metallic surfaces. *Nano Lett* 4(11):2209
14. Lassiter JB, Azipurua J, Hernandez LI, Brandl DW, Romero I, Lal S, Hafner JH, Nordlander P, Halas NJ (2008) Close encounters between two nanoshells. *Nano Lett* 8(4):1212
15. Liu N, Giessen H (2010) Coupling effects in optical metamaterials. *Angew Chem* 49:9383
16. Palik ED (ed) (1998) *Handbook of optical constants of solids*. Academic, San Diego
17. Rodger A, Norden B (1997) *Circular dichroism and linear dichroism*. Oxford University Press, Oxford
18. Maier SA (2007) *Plasmonics: fundamentals and applications*. Springer Publishers, New York
19. Svirko YP, Zheludev NI (1998) *Polarization of light in nonlinear optics*. Wiley Press, New York
20. Born M (1915) The natural optical activity of liquids and gases. *Phys Z* 16:251
21. Yin X, Schaferling M, Metzger B, Giessen H (2013) Interpreting chiral nanophotonic spectra: the plasmonic Born-Kuhn model. *Nano Lett* 13(12):6238